THE JOURNAL OF PHYSICAL CHEMISTRY B

Article

pubs.acs.org/JPCB

Grand Canonical Monte Carlo Simulations Guided by an Analytic Equation of State—Transferable Anisotropic Mie Potentials for Ethers

Andrea Hemmen,[†] Athanassios Z. Panagiotopoulos,[‡] and Joachim Gross*,[†]

[†]Institute of Thermodynamics and Thermal Process Engineering, University of Stuttgart, Pfaffenwaldring 9, 70569 Stuttgart, Germany

[‡]Department of Chemical and Biological Engineering, Princeton University, Princeton, New Jersey 08544, United States

Supporting Information

ABSTRACT: In this study, we propose using an analytical equation of state for guiding molecular simulations in the grand canonical ensemble. Molecular simulations in the grand canonical ensemble deliver phase equilibrium properties with low statistical uncertainty. The entire phase envelope can be obtained when histograms of several simulations along the phase envelope are combined. In this study, we explore the use of an analytical equation of state for defining chemical potentials, temperatures, and intervals of molecule numbers for simulations in the grand canonical ensemble, such that the phase envelope is traced. We limit particle numbers to intervals and ensure even sampling of molecule numbers in each interval by applying a bias potential determined from transition-matrix sampling. The methodology is described for pure components and binary mixtures. We apply the simulation method to develop parameters of the transferable anisotropic Mie (TAMie) force field for ethers. We find that the partial charges optimized individually for diethyl ether and for dipropyl ether differ substantially from the partial charges optimized simultaneously to both substances. The concept of transferable partial charges is thus a significant assumption. For developing the (TAMie) force field, we constrained the partial charge to a range, where individually optimized partial charges were found.

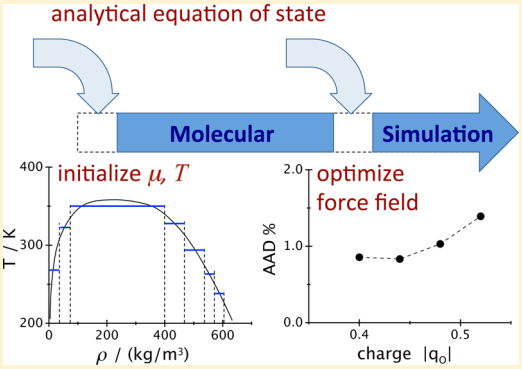

INTRODUCTION

Monte Carlo simulations in the grand canonical ensemble (GCMC) are suitable for calculating phase equilibria of fluids. Accurate data for the phase equilibrium properties in the vicinity of critical points can be generated from a single simulation run, provided suitable values of temperature T and chemical potentials μ_i of all species are specified.[1−4] During a GCMC simulation, a histogram $H(N, E)$ of finding the system with N molecules and with the energy E is collected and the phase equilibrium calculation occurs a posteriori using histogram reweighting to determine the precise conditions at which equality of pressure and chemical potentials of all components occur in the coexisting phases. Histogram reweighting allows for determining the probability distribution (histogram) for other conditions T' and μ_i' sufficiently close to the condition T and μ_i specified in the GCMC simulation. The phase equilibrium can thus be traced for various temperatures T' (close to T) by determining a value of μ_i' that satisfies equal pressure in both phases. An elegant approach for obtaining the entire phase envelope of a pure component is given by combining the histograms of several GCMC simulations conducted at $\{T, \mu_i\}$ conditions along the phase envelope.[5−9]

A key barrier to application of the multiple-histogram approach is the lack of *a priori* knowledge of suitable $\{T, \mu_i\}$ conditions to be specified along a phase envelope. This is often circumvented by starting with simulations in the vicinity of the critical point and determining $\{T, \mu_i\}$ estimates for successive GCMC runs at lower temperature from preliminary phase equilibrium calculations. Instead of this iterative approach, in this study, we suggest using analytical equations of state for estimating suitable $\{T, \mu_i\}$ conditions.

For a review of histogram reweighting techniques as well as on other methods for determining phase equilibrium properties, such as the Gibbs ensemble, the *NPT*-test particle method, and Gibbs−Duhem integration, we refer to articles by Panagiotopoulos,[10] de Pablo et al.,[1] and Guevara-Carrion et al.[11]

During Monte Carlo simulations, one collects data on visited states along a Markov chain and calculates averages. Transition-matrix sampling[12−17] offers an alternative to visited-states approaches. Transition-matrix collects data on attempted transitions, which on the one hand leads to very precise results. On the other hand, the approach is versatile for problems where a regular importance-sampling scheme would unlikely "by itself" visit certain states. In these cases, a system is

Received: February 23, 2015
Revised: May 11, 2015
Published: May 11, 2015

DOI: 10.1021/acs.jpcb.5b01806
J. Phys. Chem. B 2015, 119, 7087−7099

given an incentive (bias) to move into certain states, or it is simply constrained to visit a certain state.[18]

Errington[19] developed a transition-matrix scheme for calculating vapor−liquid phase equilibrium properties from molecular simulations in the grand canonical ensemble. A bias function is calculated on the fly that leads to a flat histogram along the coordinate of molecule numbers N and permits passing the large energy barrier between vapor and liquid phase.

The straightforward sampling of molecular insertions or deletions in open ensembles or the sampling of trial insertions for calculating chemical potentials suffers from poor statistics at high densities and for larger molecules. Transition-matrix sampling can be used to improve the statistical accuracy of these moves. Fenwick and Escobedo[20] showed the transition-matrix sampling to be closely related to Bennett's optimized acceptance ratio method.[21] Transition-matrix sampling is particularly suited for extended ensemble simulations.[22] Shi and Maginn proposed a staged insertion and deletion scheme, referred to as continuous fractional component MC, where not only neighboring states in the stage-wise insertion of a molecule are allowed.[23] They achieved good sampling of molecule transfer moves for mixtures involving ionic liquids.[24]

Shen and Errington also used transition-matrix sampling for calculating phase equilibrium properties of binary and ternary mixtures.[25] They studied a number of model binary Lennard-Jones systems to validate the methodology and showed that the entire vapor−liquid phase diagram can be calculated from results of a single simulation using histogram reweighting. Furthermore, Errington and Shen[26] presented an approach for directly locating phase transitions in multicomponent systems and showed promising results for mixtures with asymmetry of both, size and energy parameters of the species.

In previous work of our group, Sanchez et al.[27] used the PC-SAFT equation of state[28] to estimate a weight function, which allows a system to overcome the energetic barrier between vapor and liquid phase. The possibility of using an analytical equation of state for supporting molecular simulations has earlier and very generally been worked out by Gospodinov and Escobedo.[29] They very convincingly showed that probability distributions in various ensembles can be estimated by equations of state.[29,30] The interplay between molecular simulations and fluid theories is therefore not any more a one-way relation, namely, that molecular simulations allow systematic evaluation and parametrization of fluid theories. Gospodinov and Escobedo[29,30] showed that molecular simulations can much benefit from applications of fluid theories, for example, by providing weight functions for non-Boltzmann simulations.

The utility of analytic fluid theories in obtaining force fields to be used in molecular simulation studies is impressively demonstrated by the group at Imperial College in London. They use the SAFT-γ model[31−33] for determining force field parameters of coarse grained molecular models. The approach was successfully shown for carbon dioxide,[34] greenhouse gas species, refrigerants and alkanes,[35] as well as for aromatic hydrocarbons.[36] The coarse grained models allow for efficient and accurate simulations of large-scale problems, such as micellar structures, as Müller and Jackson show.[37] The utility of fluid theories for molecular simulations has also been established in the group of Elliott, where transferable intermolecular potentials for organic species were developed on the basis of perturbation theory,[38,39] and where fluid theory was shown to predict results of molecular simulations of homogeneous systems[40] and interfaces.[41] In other previous work, van Westen et al. showed that the iteration of force-field parameters becomes very efficient with the help of an analytic equation of state.[42] The analytic equation of state (PC-SAFT) is first expressed in terms of the force-field parameters. It is then adjusted to the outcome of molecular simulations. In a next step, the model can be used for optimizing the force field parameters toward experimental data. The predictions of the equation of state are only approximate, which is why the procedure is iterative. The convergence however is rapid; three to five iteration steps are typically sufficient for the simultaneous iteration of four van der Waals force-field parameters.[42,43] A modification of the algorithm was proposed in our previous study. It was shown that a converged state according to the analytic equation of state indeed minimizes the true objective function; i.e., the approximations and errors caused by the equation of state do not affect the objective function at the minimum.[43]

This study has two objectives. It describes an implementation of GCMC simulations with histogram reweighting that allows determination of the entire vapor−liquid phase envelope from a single run. The N-domain, where N denotes the number of molecules, is divided into windows of widths ΔN that run in parallel, leading to a time efficient simulation scheme. The windows are defined at different temperatures and chemical potentials, such that the phase equilibrium curve of the considered system is traced. The PC-SAFT equation of state is used to define suitable temperature and chemical potentials. Second, this study extends the parametrization of the transferable anisotropic Mie potential (TAMie) force field[43] considering the functional group of ethers. These force field parameters are adjusted to liquid densities and to vapor pressures, and the results show good agreement with experimental data.

SIMULATION METHOD: PURE COMPONENTS

Monte Carlo simulations are here conducted in the grand canonical ensemble (GCMC), where the excess chemical potentials μ, volume V, and temperature T are specified, whereas the molecule number N and energy E fluctuate. The excess chemical potential is defined as the total chemical potential, where the de Broglie wavelength $\Lambda(T)$ (that here contains intramolecular degrees of freedom) is removed, according to $\mu = \mu^{tot} - k_B T \ln(\Lambda^3)$, with k_B as Boltzmann's constant. For brevity, we omit the word "excess" henceforth. All static thermodynamic quantities can immediately be determined for the defined variables $\{\mu, T\}$. Histogram reweighting, however, also allows calculating thermodynamic quantities for other temperatures and other chemical potentials in the vicinity of the specified values. With histogram reweighting techniques, one can determine the entire phase envelope, provided multiple $\{\mu_i, T_i\}$ conditions are sampled, such that a probability distribution for states around the phase envelope can be constructed.[6−9] Defining suitable $\{\mu_i, T_i\}$ conditions that approximately trace the phase envelope is somewhat tedious, since the chemical potential that approximately leads to phase equilibrium conditions for a given T is not known *a priori*. We propose to use an analytic equation of state, such as the PC-SAFT equation of state,[28] for providing suitable estimates for $\{\mu_i, T_i\}$ conditions.

The procedure is as follows: We determine the critical temperature T_{est}^c of the pure component of interest according to PC-SAFT. Then, 10 subcritical temperatures T_i are calculated

DOI: 10.1021/acs.jpcb.5b01806
J. Phys. Chem. B 2015, 119, 7087−7099

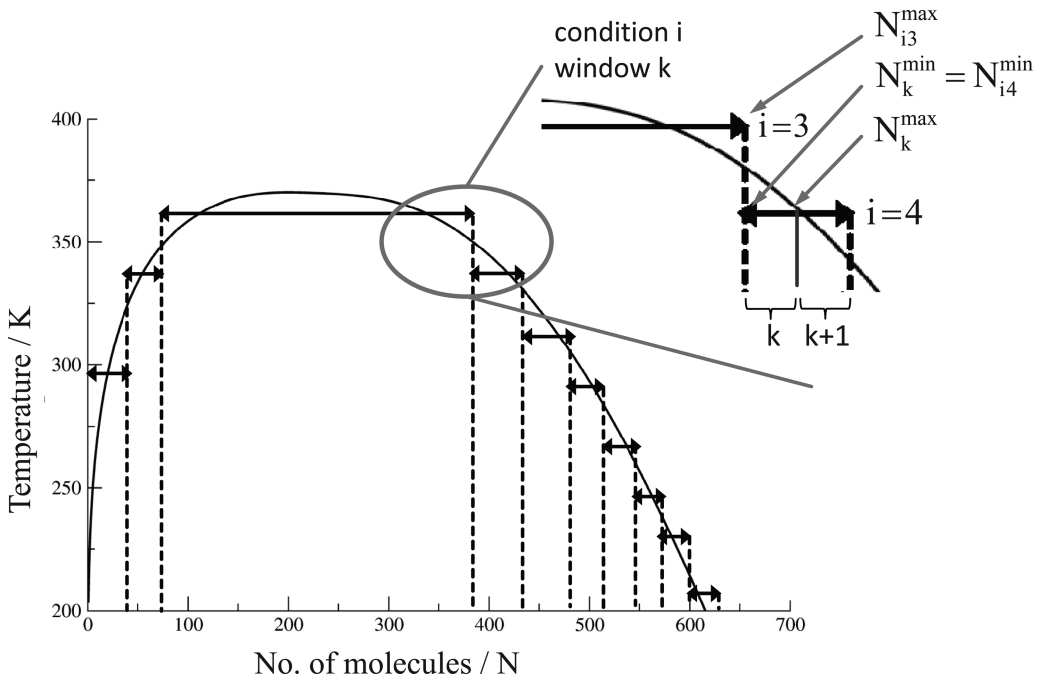

Figure 1. Tracing the vapor−liquid equilibrium with suitable $\{\mu_i, T_i\}$ conditions visualized as double arrows. A condition is defined for a range of molecule numbers and is further subdivided into windows of $\Delta_k N$. Conditions overlap at the bonds with $N_i^{max} = N_{i+1}^{min}$.

such that a vapor−liquid equilibrium curve is traced as shown schematically in Figure 1, with a lowest temperature of $0.55T_{est}^{c}$. We use the terminology "condition" i for the specifications $\{\mu_i, T_i\}$ that are visualized as a horizontal double arrow in Figure 1. A condition is specified for a defined range of molecule numbers, as $N_i^{min} \leq N \leq N_i^{max}$. The first two conditions $i = 1, 2$ sample the vapor phase, the third condition with temperature T_3 approximately spans the critical region, while all further conditions sample the liquid phase. From PC-SAFT, we determine the temperature conditions T_i, the chemical potentials μ_i, and the range of molecule numbers. In order to later connect the simulation results at one condition i to the next condition $i + 1$, the upper bound of the molecule number N_i^{max} is also sampled as a lower bound of the interval $N_{i+1}^{min} = N_i^{max}$, as illustrated in Figure 1. The interval of molecule numbers (N_i^{min} to N_i^{max}) is further subdivided into windows of, say, $\Delta N_k = 5$, where k is an index counting the windows.[44] Dividing the problem into small windows is advantageous, because suitable simulation parameters, such as maximum displacement or number of configurational bias steps, are trivially defined for a narrow range of molecule numbers. However, more importantly, the calculation time for each window is low and all windows run in parallel.

Multiple Histogram Sampling Using Transition-Matrix Sampling. GCMC simulations are executed for all conditions $i \in [1, ..., 10]$ collecting histograms of the form $H_i^{bias}(N, E)$. We use transition-matrix sampling in order to more evenly and more accurately sample the N-space in each GCMC simulation. The transition-matrix method allows defining a bias potential, which leads to even sampling along the N-coordinate. We collect simple "visited state" histograms $H_i^{bias}(N, E)$ and use the probability distribution from the transition-matrix scheme in order to obtain an unbiased probability distribution $H_i(N, E)$. Transition-matrix sampling gives very accurate distributions along the N-coordinate, because it is based on transition probabilities, and not on visited states. Using a bias potential from transition-matrix sampling offers another advantage in the postprocessing step, where the histogram $H_{i+1}(N, E)$ will be connected to the neighboring histogram $H_i(N, E)$: In our scheme, histograms are connected at a predefined switchover point at $N_{i+1}^{min} = N_i^{max}$, which is well-sampled from both sides as a result of the bias potential. As a postprocessing step, we apply a histogram reweighting scheme, first, to connect all distributions $H_i(N, E)$ and, second, to calculate phase equilibrium properties.

GCMC simulations of all windows are initiated in parallel. The windows in molecule number are chosen of width ΔN_k = 10 and 5 for lower densities and for higher densities, respectively. Any trial insertion of a molecule into the system that would exceed the upper limit in molecule number of a window, N_k^{max}, is trivially rejected. Analogously, any molecular deletion move, when $N = N_k^{min}$ is immediately rejected. Virnau et al. showed that the statistical error of a combined probability distribution does not depend on the choice of the window width.[44]

Histograms $H_k^{bias}(N, E)$ of all windows k are collected by discretizing the energy into energy bins of width ΔE, ranging from E_λ to $E_{\lambda+1} = E_\lambda + \Delta E$. The lowest and highest anticipated energies $E_{\lambda=0}$ and $E_{\lambda^{max}}$ defined for an entire window k, respectively, are determined in the equilibration phase of the simulation. During the production phase of the GCMC simulation, the histogram is updated after every Monte Carlo (trial) move: for a certain state $\{N, E\}$, the appropriate bin λ of the histogram into which E falls is augmented by unity, as $H_i^{bias}(N, E_\lambda) \doteq H_i^{bias}(N, E_\lambda) + 1$. In order to simplify the notation, we henceforth write $H_i^{bias}(N, E)$, omitting the index λ. Further, for a summation over all entries in the energy distribution for a given N, we use the shorthand notation $\sum_E H_i^{bias}(N, E)$, rather than specifying the index over which the summation runs.

The transition-matrix method allows generating a bias function on the fly, ensuring uniform sampling of the N-coordinate. Collecting entries in the transition matrix is

DOI: 10.1021/acs.jpcb.5b01806
J. Phys. Chem. B 2015, 119, 7087−7099

detached from the acceptance rules of the Markov chain, so that all of the samples taken remain valid, regardless of whether a bias potential is already applied in the simulation or not. In the context of GCMC simulations, the transition-matrix scheme was in detail described and analyzed by Errington.[19] One sums the probabilities of attempted transitions between states in a collection matrix with elements $C_{N\to N+1}$, $C_{N\to N}$, and $C_{N\to N-1}$ which is updated after each Monte Carlo step. For a trial addition of a molecule, two elements of the collection matrix are augmented as

$$C_{N\to N+1} \doteq C_{N\to N+1} + \pi^{\text{accept}}_{N\to N+1} \tag{1}$$

$$C_{N\to N} \doteq C_{N\to N} + (1 - \pi^{\text{accept}}_{N\to N+1}) \tag{2}$$

where $\pi^{\text{accept}}_{N\to N+1}$ is the probability of an unbiased system to make a transition from N molecules to a state with $N + 1$ molecules. The dot above the equal sign in these equations indicates algorithmic equations for updating a quantity, rather than a strictly mathematical equality. The elements of the collection matrix are augmented irrespective of whether the trial move is accepted or not. For a trial deletion move, the above scheme is analogous and is obtained by replacing the positive sign in all subscripts of eqs 1 and 2 by a negative sign. The unbiased acceptance probabilities for the insertion and deletion of a molecule are

$$\pi^{\text{accept}}_{N\to N+1} = \min\left[1, \frac{V}{N+1}\exp(-\beta\Delta E + \beta\mu)\right] \tag{3}$$

$$\pi^{\text{accept}}_{N\to N-1} = \min\left[1, \frac{N}{V}\exp(-\beta\Delta E - \beta\mu)\right] \tag{4}$$

where $\beta = (k_B T)^{-1}$ denotes the inverse temperature. For thermal fluctuation moves, such as translation, rotation, and reconfiguration moves, the only augmented element of the collection matrix is

$$C_{N\to N} \doteq C_{N\to N} + 1 \tag{5}$$

The transition probability can then be calculated as

$$P_{N\to N+\delta} = \frac{C_{N\to N+\delta}}{C_{N\to N+1} + C_{N\to N} + C_{N\to N-1}} \tag{6}$$

where $\delta \in \{+1, 0, -1\}$ is used to indicate state changes with increasing molecule number, constant molecule number, and decreasing molecule number, respectively. Detailed balance relates the probability $P(N)$ to be in a state with N molecules to the probability $P(N + 1)$ of finding the unbiased system in a state with $N + 1$ molecules, as

$$P(N+1) = P(N)\frac{P_{N\to N+1}}{P_{N+1\to N}} \tag{7}$$

We first set $P(N = N^{\min}_k) = 1$, which leads to a non-normalized probability distribution. Equation 7 is then used recursively to obtain the probability $P(N)$ for the entire range of N of the considered window.

Bias Potential from Transition Matrix. The probability distribution $P(N)$ makes it possible to define a biasing function

$$w(N) = -\ln P(N) \tag{8}$$

which enables even sampling of all molecule numbers in the considered range of applicability.[4,19,27] Probabilities for accepting a trial insertion and a trial deletion of a molecule are

$$\pi^{\text{accept,bias}}_{N\to N+1} = \min\left[1, \frac{V}{N+1}\exp(-\beta\Delta E + \beta\mu + \Delta w)\right] \tag{9}$$

$$\pi^{\text{accept,bias}}_{N\to N-1} = \min\left[1, \frac{N}{V}\exp(-\beta\Delta E - \beta\mu + \Delta w)\right] \tag{10}$$

where the Δ-operator defines the difference of trial state minus current state.

Postprocessing: Combining Histograms. After completion of the GCMC simulations of all windows, one can combine the individual probability distributions to one single probability distribution, which is used to calculate equilibrium properties. Combining the probability distribution is done in two steps: first, the histograms $H^{\text{bias}}_k(N, E)$ of all windows k within one $\{T_i, \mu_i\}$ condition i are scaled with the probability $P_i(N)$ from transition-matrix sampling, which removes the bias and leads to histograms $H_i(N, E)$ for the entire range of condition i. Second, all histograms $H_i(N, E)$ are combined to a single distribution.

The N-coordinate of a condition i is in general subdivided into windows of a certain range, from $N^{\min}_k$ to $N^{\max}_k$ (as shown in Figure 1). Let us consider the case, where five windows $\{k1, ..., k5\}$ are present for condition i. We first set $P_i(N = N^{\min}_{k1}) = 1$, where $N^{\min}_{k1}$ is the left-most molecule number of condition i. Equation 7 is then applied recursively to obtain $P_i(N)$ for the entire range of the condition. The molecule number thereby runs from $\{N^{\min}_{k1}, ..., (N^{\max}_{k1} - 1), N^{\min}_{k2}, ..., ... (N^{\max}_{k5} - 1)\}$. Note that $P_i(N)$ is so far the non-normalized probability distribution.

The unbiased histogram is obtained by scaling the biased histogram with the probability distribution from transition-matrix sampling, according to

$$H_i(N, E) = \frac{H^{\text{bias}}_i(N, E)}{\sum_E H^{\text{bias}}_i(N, E)} P_i(N) \tag{11}$$

for all molecule numbers N and energies E within a $\{T_i, \mu_i\}$ condition. The last remaining step is to combine the probability distributions $H_i(N, E)$ of all conditions to a unified probability distribution. The basis for attaching various probability distributions is histogram reweighting. The multiple histogram method was established by Ferrenberg and Swendsen[5] and Panagiotopoulos et al.[8] and is based on connecting histograms from different conditions iteratively such that the predicted and observed histograms are closest. In our application, the probability distributions do not overlap for several values of N. Rather, the switchover from one condition to the next occurs at a single value of N. The use of a bias potential in the acceptance rule ensures even sampling along the N-coordinate within each condition. As a consequence, the switchover from one condition to the next is well sampled and weight functions proposed by Ferrenberg and Swendsen[5] are not needed here.

In order to better discuss histogram reweighting, we extend our notation from $H_i(N, E)$ toward $H_i(N, E; \beta_i, \mu_i)$. The basic relation of histogram reweighting is

$$H_i(N, E; \beta, \mu) = H_i(N, E; \beta_i, \mu_i) C \exp(-(\beta - \beta_i)E + N(\beta\mu - \beta_i\mu_i)) \tag{12}$$

with $C = \Xi(\mu_i, V, \beta_i)/\Xi(\mu, V, \beta)$ as the ratio of the grand canonical partition functions. If H_i is summed over all energy bins, as $\sum_E H_i(N, E; \beta, \mu)$, one gets the (non-normalized) probability of finding a system with N molecules for any pair of

DOI: 10.1021/acs.jpcb.5b01806
J. Phys. Chem. B 2015, 119, 7087−7099

$\{\beta, \mu\}$, not too far from the sampled condition $\{\beta_i, \mu_i\}$. The histograms of two neighboring conditions i and $i+1$ are simply attached by requiring this probability to be the same for an average inverse temperature $\overline{\beta} = (\beta_i + \beta_{i+1})/2$ and at an average chemical potential $\overline{\beta\mu} = (\beta_i\mu_i + \beta_{i+1}\mu_{i+1})/2$, so that

$$H_{i+1} \doteq H_{i+1}\frac{\sum_E H_i \exp(-(\overline{\beta} - \beta_i)E + N(\overline{\beta\mu} - \beta_i\mu_i))}{\sum_E H_{i+1} \exp(-(\overline{\beta} - \beta_{i+1})E + N(\overline{\beta\mu} - \beta_{i+1}\mu_{i+1}))} \tag{13}$$

where $H_i = H_i(N, E; \beta_i, \mu_i)$ and $H_{i+1} = H_{i+1}(N, E; \beta_{i+1}, \mu_{i+1})$ and N as the switchover point of the two conditions as illustrated in Figure 1. Equation 13 is again an algorithmic equation for updating H_{i+1}, as the dot over the equal sign indicates. This equation factors the ratio of two a priori unknown "constants" C of eq 12 into H_{i+1} (along with another constant that is due to the non-normalized scale of the probability distributions). Once eq 13 is applied recursively for all conditions i, one has the entirely connected non-normalized probability distribution $H(N, E; \beta, \mu)$.

Phase Equilibrium Conditions from Histogram Reweighting. Histogram reweighting is now applied to obtain vapor−liquid equilibrium properties, and a mixed field scaling approach is used to estimate the critical properties. The probability distribution of finding N molecules (regardless of the energy) given a chemical potential μ and inverse temperature β is obtained by summing eq 12 over all energy states and by normalizing, according to

$$P(N; T, \mu) = \frac{\sum_E H(N, E; \beta_j, \mu_j) \exp(-(\beta - \beta_j)E + N(\beta\mu - \beta_j\mu_j))}{\sum_N \sum_E H(N, E; \beta_j, \mu_j) \exp(-(\beta - \beta_j)E + N(\beta\mu - \beta_j\mu_j))} \tag{14}$$

here, j is a generic index for the condition into which a given N falls. For the phase equilibrium calculations, we specify a temperature T and determine the corresponding chemical potential $\mu^{coex}(T)$ by requiring equal pressure in the vapor and liquid phase. For a phase equilibrium condition, the probability distribution $P(N; T, \mu^{coex}(T))$ is bimodal with a vapor peak for molecule numbers corresponding to a vapor phase and a liquid peak at higher number of molecules. The same pressure is ensured when the sum $I^{vap} = \sum_{N=0}^{N^{div}} P(N; T, \mu^{coex}(T))$ under the vapor peak is equal to the corresponding sum, I^{liq}, for the liquid peak. The local minimum in the probability distribution $P(N^{div}; T, \mu^{coex}(T))$ between the two peaks at molecule number N^{div} defines the upper and lower summation limits for the vapor and the liquid phase, respectively. We use a Newton scheme for finding the root $f(\mu^{coex}) = 0$ of the function $f(\mu^{coex}) = \ln(I^{vap}/I^{liq})$ using finite differences with eq 14. The logarithmic definition of the target function leads to robust convergence in a few steps only. For the converged distribution $P^{coex}(N; T) = P(N; T, \mu^{coex}(T))$, we can calculate thermodynamic averages of a static property A, as

$$\langle A\rangle^{vap} = \sum_{N=0}^{N^{div}} 2P^{coex}(N; T)A(N) \tag{15}$$

$$\langle A\rangle^{liq} = \sum_{N=N^{div}}^{N^{max}} 2P^{coex}(N; T)A(N) \tag{16}$$

The factor 2 in these equations appears because the probability distribution is normalized for two coexisting phases. The vapor pressure is obtained from formulating the probability density of a grand canonical ensemble for the ideal gas limit at $N = 0$, according to

$$p^{sat}(T) = -\frac{k_B T}{V}\ln(2P^{coex}(N = 0; T)) \tag{17}$$

For determining the pure components' critical point, we apply the mixed-field scaling approach. One uses the universal scaling laws characterizing the critical point as a second-order phase transition to relate the critical behavior of a molecular fluid to the critical behavior of the 3D-Ising model.[45] The approach is well documented, and we refer to the review of Wilding[46] and the review of Panagiotopoulos.[2]

Mixed-field scaling is here realized by defining an order parameter

$$M = \alpha_1(N - \alpha_2\langle E\rangle_N - \alpha_3) \tag{18}$$

The regression of the unknown parameters is done using a Levenberg−Marquardt algorithm by minimizing the sum $\sum_N \tau(N)^2$ of squared deviations, defined as

$$\tau(N) = \ln\left(\frac{P^{Ising}(M)}{\alpha_4 \cdot P^{coex}(N)}\right)\omega(M) \tag{19}$$

with the empirical weight function $\omega(M)$ emphasizing the range of the order parameter of importance to the critical scaling

$$\omega(M) = \begin{cases} 10/(-\ln(P^{Ising}(M)))^2 & \text{for } P^{Ising}(M) > 10^{-5} \\ 0 & \text{for } P^{Ising}(M) \le 10^{-5} \end{cases}$$

Six degrees of freedom are determined by the minimization, namely, α_1 to α_4, the critical temperature T^{crit}, and the corresponding chemical potential μ^{crit}. Good starting values can be defined ensuring a robust convergence of the mixed field scaling regression, provided an initial guess for T^{crit} and μ^{crit} is available. We obtain these initial values by increasing the temperature in steps of 1 K, each time adjusting μ such that the two characteristic peaks in $P(N)$ at $(N_{peak})^{low}$ and $(N_{peak})^{high}$, at low and high molecule numbers, respectively, are of equal height. We end this temperature scan when the probability distribution roughly resembles the appropriate critical distribution of the 3D-Ising model; i.e., we stop once the local minimum (occurring at N^{div}) between the two peaks is roughly 0.43 times the peak height. The starting values for the four parameters α_1−α_4 are then chosen as

$$\alpha_1 = 2.2((N_{peak})^{high} - (N_{peak})^{low})^{-1} \tag{20}$$

$$\alpha_2 = 0 \tag{21}$$

$$\alpha_3 = N^{div} \tag{22}$$

$$\alpha_4 = 0.3(N_{peak})^{high} \tag{23}$$

The iteration of the critical point for pure components converged reliably to average square deviations (eq 19) of order $<10^{-4}$ for all cases considered here.

DOI: 10.1021/acs.jpcb.5b01806
J. Phys. Chem. B 2015, 119, 7087−7099

SIMULATION METHOD: BINARY MIXTURES

For mixtures, we also apply a transition-matrix sampling scheme and use histogram reweighting to determine vapor−liquid (and liquid−liquid) equilibria. Suitable simulation conditions of molecule numbers $\mathbf{N} = (N_1, N_2)$ and excess chemical potentials $\boldsymbol{\mu} = (\mu_1, \mu_2)$ are estimated with the PC-SAFT equation of state.[28] The chemical potentials should be estimates of the chemical potentials at a representative equilibrium point. In practice, we choose a pressure condition somewhere in the middle of the anticipated phase diagram of interest and determine the chemical potentials from the PC-SAFT model. The exact value is not important, but the values of $\boldsymbol{\mu}$ scale the weights in transition-matrix sampling, as will be shown below. An example for the $\mathbf{N}$-space as calculated from PC-SAFT and as obtained from molecular simulations is illustrated in Figure 2 for a given volume V and temperature T.

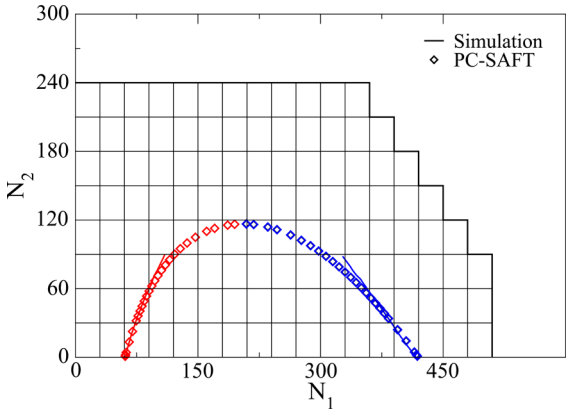

Figure 2. N_1−N_2 sampling area of the methane−butane mixture at T = 394.26 K. The compositions of vapor and liquid phase at different pressures are calculated with PC-SAFT (diamonds) and GCMC simulation (line).

For mixtures, we construct the result of a GCMC simulation by performing individual MC simulations, where the molecule numbers N_1 and N_2 of both species are not allowed to freely fluctuate. Rather, we consider mixtures in multiple canonical ensembles for each relevant point in (N_1, N_2) space and construct a probability surface, as would be obtained from a GCMC simulation. This could be realized by performing individual simulations for all (N_1, N_2) points. In our case, we define rectangular windows of $(\Delta N_1, \Delta N_2)$ (as indicated in Figure 2), where all (N_1, N_2) points are successively visited for an exactly defined number of Monte Carlo cycles. The Monte Carlo cycles for an (N_1, N_2) point comprise thermal fluctuation moves (translation, rotation, reconfiguration) as well as never accepted "trial insertions" and never accepted "trial deletions". Only after completion of all MC cycles, the (N_1, N_2) point is left toward a neighboring, say, $(N_1 + 1, N_2)$ point. This way, the system moves stepwise meandering through the simulation window and samples each (N_1, N_2) combination with a defined number of Monte Carlo steps. This procedure represents a by-definition flat-histogram method. Each window $(\Delta N_1, \Delta N_2)$ is calculated on a compute node and all windows run in parallel, leading to short calculation times.

Transition-Matrix Sampling. Like for pure components, the probabilities of attempted transitions are summed in a collection matrix with elements such as $C_{N_1,N_2\to N_1+1,N_2}$, for example.[25,26] The transition probabilities are calculated analogous to eq 6. Note that the estimated chemical potentials enter into the sampling results via eqs 3 and 4 (only now formulated for mixtures). We observe that a rough estimate of the chemical potentials for mixtures as obtained from PC-SAFT is sufficient to produce reliable results. The probability $P(N_1, N_2)$ of finding a system in a state with N_1 and N_2 molecules is again obtained from detailed balance. We use a two-step procedure. First, probabilities for the molecule range along the lower and left edge of a particle window are determined as

$$P(N_1 + 1, N_2) = P(N_1, N_2)\frac{P_{N_1,N_2\to N_1+1,N_2}}{P_{N_1+1,N_2\to N_1,N_2}} \qquad N_1 = 0 \ldots N_{1,\max} \qquad N_2 = 0 \tag{24}$$

$$P(N_1, N_2 + 1) = P(N_1, N_2)\frac{P_{N_1,N_2\to N_1,N_2+1}}{P_{N_1,N_2+1\to N_1,N_2}} \qquad N_1 = 0 \qquad N_2 = 0 \ldots N_{2,\max} \tag{25}$$

which corresponds to the x- and y-axis of Figure 2. $N_{i,\min}$ and $N_{i,\max}$ are the minimum and maximum particle numbers for species i. For all remaining molecule numbers, the probability is calculated from

$$P(N_1, N_2) = \frac{1}{2}\left(P(N_1 - 1, N_2)\frac{P_{N_1-1,N_2\to N_1,N_2}}{P_{N_1,N_2\to N_1-1,N_2}} + P(N_1, N_2 - 1)\frac{P_{N_1,N_2-1\to N_1,N_2}}{P_{N_1,N_2\to N_1,N_2-1}}\right) \tag{26}$$

Phase Equilibrium Conditions from Histogram Reweighting. Histogram reweighting[5] is applied to obtain vapor−liquid equilibrium or liquid−liquid equilibrium properties. We now extend the notation again from $P(N_1, N_2)$ to $P(\mathbf{N}; \beta, \boldsymbol{\mu})$, in order to indicate that the probability was determined for estimated chemical potentials $\boldsymbol{\mu}$ and for inverse temperature β. A rescaling of inverse temperature β is here not considered, so that from eq 12 applied to mixtures, we simply get

$$P(\mathbf{N}; \beta, \boldsymbol{\mu}^{\text{coex}}) = P(\mathbf{N}; \beta, \boldsymbol{\mu}) \exp[\mathbf{N}(\beta\boldsymbol{\mu}^{\text{coex}} - \beta\boldsymbol{\mu})] \tag{27}$$

where a scalar product is taken in the argument of the exponent. We note that the probability distribution needs to be normalized. For a phase equilibrium condition, we iterate the chemical potential $\boldsymbol{\mu}^{\text{coex}}$ requiring equal pressure in vapor and liquid phase. More specifically, we define one value of $\boldsymbol{\mu}^{\text{coex}}$, say, μ_1^{coex}, and iterate the other value, μ_2^{coex}, to give phase equilibrium properties. A different definition of μ_1^{coex} along with an iteration of μ_2^{coex} leads to a next equilibrium condition. The iteration requires the same pressure of both phases, so that the sum under the vapor peak $I^{\text{vap}} = \sum_{N_1,N_2}^{\text{vap}} P(\mathbf{N}; \beta, \boldsymbol{\mu}^{\text{coex}})$ must be equal to the corresponding sum I^{liq} under the liquid peak. As for the pure components, we use a Newton scheme to find the root of the function $f(\boldsymbol{\mu}) = \ln(I^{\text{vap}}/I^{\text{liq}})$. For the converged values $\boldsymbol{\mu}^{\text{coex}}$, we calculate thermodynamic properties, such as the equilibrium mole fraction of species i in phase ϕ with

$$x_i^{\phi} = \frac{\langle N_1\rangle^{\phi}}{\langle N_1\rangle^{\phi} + \langle N_2\rangle^{\phi}} \tag{28}$$

DOI: 10.1021/acs.jpcb.5b01806
J. Phys. Chem. B 2015, 119, 7087−7099

$$\langle N_i \rangle^{\phi} = \sum_{N_1,N_2}^{\phi} N_i 2P(\mathbf{N};\, T, \boldsymbol{\mu}^{\mathrm{coex}}) \tag{29}$$

The equilibrium pressure is determined from the ideal gas limit (eq 17) at $N_1 = 0$ and $N_2 = 0$.

For the determination of the critical point, we apply the Binder cummulant[47] intersection method and extrapolate the results of four different simulation volumes with finite size scaling rules to the limit of infinite volume.[48] For the critical parameters pressure p and mole fraction x_i, we use the relation $\langle p^c \rangle(L) - \langle p^c \rangle(\infty) \sim L^{-(3-1/\nu)}$ and $\langle x_i^c \rangle(L) - \langle x_i^c \rangle(\infty) \sim L^{-(3-1/\nu)}$ with the universal scaling constant $\nu = 0.6289$.[49] The Binder parameter B_L is determined as

$$B_L = \frac{\langle \mathcal{X}^4 \rangle}{\langle \mathcal{X}^2 \rangle^2} \tag{30}$$

$$\mathcal{X} = \rho - \langle \rho \rangle \tag{31}$$

For simulations with constant volume V, order parameter $\mathcal{X}$ can be expressed with molecule number N. The Binder parameter for a binary mixture is determined as

$$B_L = \frac{\sum_{N_1,N_2} ((N_1 + N_2) - \bar{N})^4 P(\mathbf{N};\, \beta, \boldsymbol{\mu}^{\mathrm{coex}})}{[\sum_{N_1,N_2} ((N_1 + N_2) - \bar{N})^2 P(\mathbf{N};\, \beta, \boldsymbol{\mu}^{\mathrm{coex}})]^2} \tag{32}$$

$$\bar{N} = \sum_{N_1,N_2} (N_1 + N_2) P(\mathbf{N};\, \beta, \boldsymbol{\mu}^{\mathrm{coex}}) \tag{33}$$

with an average molecule number $\bar{N}$ of a system in phase equilibrium. The system size dependent Binder parameter B_L is determined for all iterated phase equilibrium conditions and plotted over system pressure and concentration. The intersection of the Binder parameter is determined with the universal value at critical point $B_L = 1.6035$ for the Ising universality class.[50] The size dependent critical values are extrapolated with finite size scaling laws to obtain the critical properties.[48]

TAMIE FORCE FIELD FOR ETHER COMPONENTS

A united-atom approach is used in which carbon atoms and their adjacent hydrogen atoms are defined as a single interaction site. Similar to previous work of Toxvaerd,[51] Errington and Panagiotopoulos,[52] and Ungerer et al.,[53] the center of interaction for a CH_3 group is moved outward to better account for the effect of the hydrogen atoms. For a $CH_3(sp^3)$ group bonded to a $CH_x(sp^3)$ group, the bond length is extended by 0.2 Å to give a bond length of $r_0 = 1.54 + 0.2$ Å (see Table 1).

The total interaction potential of an interaction site is the sum of bonded and nonbonded contributions. The nonbonded potential is the sum of van der Waals pair interactions and of Coulombic potentials, as

$$u(r_{ij}) = c_{ij}\epsilon_{ij}\left[\left(\frac{\sigma_{ij}}{r_{ij}}\right)^{n_{ij}} - \left(\frac{\sigma_{ij}}{r_{ij}}\right)^{m}\right] + \frac{q_i q_j}{4\pi\epsilon_0 r_{ij}} \tag{34}$$

where the van der Waals interactions are described with a Mie potential, a generalized Lennard-Jones $(n - m)$ potential. Throughout this work, the attractive exponent is fixed to $m = 6$, as for the leading term in the expansion of dispersive energy. Excellent results for transferable force fields with a Mie potential were reported by Potoff together with Bernard-Brunel[54] and with Kamath.[55] The prefactor c_{ij} ensures a minimum value of $-\epsilon_{ij}$ for the attractive well, with

$$c_{ij} = \left(\frac{n_{ij}}{n_{ij} - 6}\right)\left(\frac{n_{ij}}{6}\right)^{6/(n_{ij}-6)} \tag{35}$$

where r_{ij} denotes the distance between two interaction sites i and j and ϵ_{ij} and σ_{ij} are the well depth and diameter parameter, respectively. Further, q_i and ϵ_0 denote the partial charge and the dielectric constant, respectively. The intermolecular potential $u(r_{ij})$ governs the interactions between united-atom groups that belong to two different molecules and between united-atom groups within one molecule that are separated by more than three bonds. Parameters for interactions between unlike types of interaction sites are determined using Lorentz–Berthelot combining rules,[56,57] as

$$\sigma_{ij} = (\sigma_{ii} + \sigma_{jj})/2 \tag{36}$$

$$\epsilon_{ij} = \sqrt{\epsilon_{ii}\epsilon_{jj}} \tag{37}$$

Mie potentials with different repulsive exponents are combined[54] according to

$$n_{ij} = (n_{ii} + n_{jj})/2 \tag{38}$$

These sets of combining rules uniquely define cross-interaction potentials. We note, however, that alternative combinations of potential functions were recently investigated by Stiegler and Sadus.[58] For the bonded force field within each molecule, we adopt a parametrization available in the literature.[59−61] We consider fixed bond lengths between the interaction sites, since bond vibrations are of high frequency and of low amplitude and their effect is unimportant for many fluid properties.[62] Bending angles between united-atom groups are generated according to the harmonic bending potential[63]

$$u_{\mathrm{bend}}(\theta) = k_\theta/2(\theta - \theta_0)^2 \tag{39}$$

with k_θ, θ, and θ_0 as the force constant, bending angle, and zero-Kelvin angle, respectively. For the torsional potential between four neighboring interaction sites, we use the OPLS-UA model,[60] according to

Table 1. Parameters of Intramolecular Potential for the TAMie Force Field, Taken from the Literature

Bond Length[59,61]		
bond type		r_0 (Å)
$CH_x(sp^3)-CH_y(sp^3)$	$x, y \in [0, 1, 2]$	1.54
$CH_3(sp^3)-CH_x(sp^3)$	$x \in [0, 1, 2]$	1.54 + 0.2
$CH_3(sp^3)-O$(ether)		1.41 + 0.2
$CH_2(sp^3)-O$(ether)		1.41

Bond Angle[59,61]		
	$x, y \in [2, 3]$	
bond type	Θ_0 (deg)	k_Θ/k_B (K)
$CH_x-CH_2(sp^3)-CH_y$	114	62500
$CH_x(sp^3)-CH_2-O$(ether)	112	50300
$CH_x(sp^3)-O$(ether)$-CH_y$	112	60400

Torsional Potential[59−61]				
torsion type	c_0/k_B (K)	c_1/k_B (K)	c_2/k_B (K)	c_3/k_B (K)
$CH_x-CH_2-CH_2-CH_y$	0	355.03	−68.19	791.32
$CH_x-CH_2-O-CH_y$	0	725.35	−163.75	558.2
$CH_x-CH_2-CH_2-O$	0	176.62	−53.34	769.93

DOI: 10.1021/acs.jpcb.5b01806
J. Phys. Chem. B 2015, 119, 7087−7099

Table 2. Parameters of the Proposed TAMie Force Field: Energy Parameter ϵ, Size Parameter σ, Repulsive Exponent n, and Point Charge q in Units of Electron Charge

pseudoatom	ϵ/k_B (K)	σ (Å)	n	q (e)
$-CH_3-$ (sp^3) all	136.318	3.6034	14	$-q_O/2$ (next to ether O)
$-CH_2-$ (sp^3) all	52.913	4.0400	14	$-q_O/2$ (next to ether O)
−O− dimethyl ether	54.36	3.213	12	$q_O = -0.35$
−O− ether	86.7	2.84	12	$q_O = -0.3$

$$u_{tor}(\phi) = c_0 + c_1[1 + \cos(\phi)] + c_2[1 - \cos(2\phi)] + c_3[1 + \cos(3\phi)] \quad (40)$$

Parameters of the TAMie force field are summarized in Tables 1 and 2. Parameters of the $CH_3(sp^3)$ and $CH_2(sp^3)$ groups are taken from Hemmen and Gross,[43] and parameters of the ether oxygen were adjusted here. The optimization algorithm is described in detail by van Westen.[42] In a recent study, we modified the algorithm and showed that, for a converged state, the equation of state does not act on the objective function.[43] The segment diameter σ_i, energy parameter ϵ_i, and point charge q_i are the three degrees of freedom for the optimization of the ether interaction site ($i = O_{ether}$). We assume the methylene groups CH_2 adjacent to the ether group to each carry a partial charge of $-q_i/2$.

SIMULATION DETAILS

Monte Carlo simulations were conducted with insertion and deletion moves, as well as translation, rotation, and partial regrow moves of molecules. A configurational bias scheme was applied, where the number of trial steps was chosen larger for N-windows at higher densities. The Mie potential is evaluated up to a radial cutoff of 14 Å with analytical long-range corrections[62,64] assuming a radial distribution function of $g(r) = 1$ beyond the cutoff distance. The electrostatic potential was evaluated with an Ewald sum, with $\kappa = 7.59L$ according to the definition given in ref 62 for a cubic box of length L and with $k_{max} = 9$ as the maximum index of the Fourier series expansion. The surface term of the Ewald sum was omitted, leading to a favorable size scaling behavior. The width of N-windows is chosen as $\Delta N = 10$ for lower densities and $\Delta N = 5$ at higher densities (i.e., for the highest 25% of molecule numbers). A total of 40 million or more MC trial steps were done for windows of $\Delta N = 10$ and 20 million trial steps or more for windows of $\Delta N = 5$. The volume of the simulation box is 40000 Å^3. No significant finite size effect was found away from the critical point for this volume.

A typical run time for a single window in the high-density region is 25 h for pure components (with partial charges) on a single core of a octa-core Intel Xeon E5−2670 processor of 2.6 GHz. About 50 parallel simulations, one for each window of molecule number, are needed to determine the complete phase envelope, whereby the windows of this high-density region limit the overall simulation time. A typical run time for a single window of the dimethyl ether/n-butane mixture in the high-density region is 13 h.

RESULTS

Pure Substances. Despite the lengthy analysis given in the previous section, the implementation of the proposed simulation method for phase equilibria of pure components and mixtures is simple in practice. A summary of the calculation steps with references to the equations of this article is given as Supporting Information. Our implementation is largely automated: the PC-SAFT equation of state is used to generate the simulation conditions in $\{T_i, \mu_i\}$, as shown in Figure 1. The output can be read by the Monte Carlo code. The Monte Carlo program processes all N-windows in a trivial parallelization using MPI. The output of the Monte Carlo simulation is a collection of histograms $H_i^{bias}(N, E)$ and the probability $P_i(N)$ from eqs 6 and 7. Both $H_i^{bias}(N, E)$ and $P_i(N)$ enter eq 11. Our implementation of the postprocessing calculation determines both the phase equilibrium points and subsequently the critical point of the fluid.

In the Supporting Information, we demonstrate that phase equilibrium properties determined from the simulation method outlined above are rather robust toward $\{\mu_i, T_i\}$ estimates from an analytic equation of state. The phase equilibrium calculations are applied in the following subsections to optimize force field parameters for ethers. The objective function for the optimization is defined in all cases as the sum of squared deviations (RMS: root-mean-square deviation) for simulated vapor pressure and liquid density data toward experimental data. Vapor pressure data and liquid density data are thereby considered with equal weight. In the following discussion and diagrams, we present absolute average deviations (AADs), because the AAD values are in our view more intuitively assessed than RMS values. The discussion and conclusions are not altered by this choice.

Dimethyl Ether. We first investigate dimethyl ether, because a detailed study on a force field parametrization of dimethyl ether for phase equilibrium properties and radial distribution functions has been performed by Ketko and Potoff.[65] Their work revealed some degeneracy in the force field parametrization, such that several combinations of the Lennard-Jones parameters $\{\epsilon_O, \sigma_O\}$ and partial charge q_O for the oxygen atom (index "O") of dimethyl ether all gave good results for critical points and phase equilibrium properties. The parameters for the CH_3 group were in their work taken from the TraPPE force field, with (positive) charges $q_{CH_3} = -0.5q_O$ placed at the center of both CH_3 groups.

It is interesting to examine whether the TAMie force field for the CH_3 group together with our definition of the objective function also leads to degeneracy of force field parameters, so that several parameter combinations give good results. We have therefore defined some fixed sets of partial charge values and simultaneously optimized the remaining Mie potential parameters $\{\epsilon_O, \sigma_O\}$. In one series of calculations, the repulsive exponent n_O of the Mie potential was set to a value of $n_O = 12$, corresponding to a Lennard-Jones (plus point charge) site for ether oxygen. A second series was conducted for $n_O = 14$ for ether oxygen, because this value was shown to best reproduce alkanes.

Figure 3 shows average deviations of simulated vapor pressure and liquid density data to experimental data[66] after optimizing the two parameters ϵ_O and σ_O. The minimum is somewhat shallow, indicating strong correlation of the three

DOI: 10.1021/acs.jpcb.5b01806
J. Phys. Chem. B 2015, 119, 7087−7099

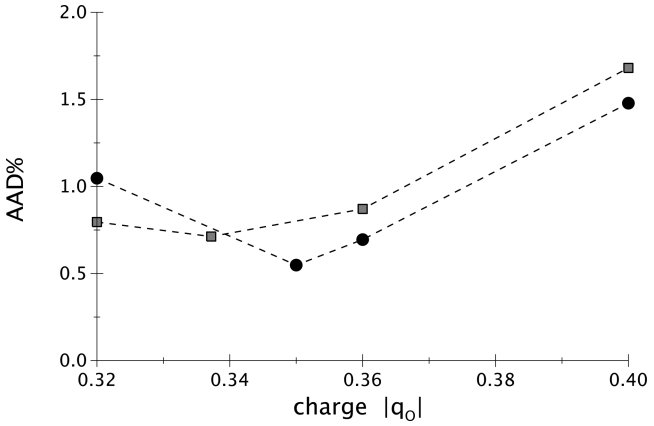

Figure 3. Dimethyl ether: Absolute average deviations (%) of simulated vapor pressure and liquid density data to experimental data for varying partial charge q_O of the oxygen. The temperature range corresponds to $0.56 \leq T/T_{crit}^{exp} \leq 0.96$. The symbols are for the case of $n_O = 12$ (spheres) and $n_O = 14$ (squares) as the repulsive Mie exponent after optimizing the two parameters ϵ_O and σ_O.

parameters. The minima, however, are nonetheless clearly identifiable. With $n_O = 12$ as the repulsive Mie exponent of the oxygen, we get an optimal value of $q_O = -0.35$; for $n_O = 14$, the best agreement is found for $q_O = -0.335$. On the basis of the results of Figure 3, we propose a parametrization with $n_O = 12$ (i.e., a Lennard-Jones site plus charge) for the ether oxygen for two reasons: First, the case of $n_O = 12$ gives lower deviations to experimental data, as Figure 3 shows. Second, the value of $q_O = -0.35$ meets the vacuum value for dimethyl ether, which is $q_O = -0.35$. An absolute effective partial charge can be somewhat higher than a vacuum value due to the static polarizability of fluids, but an effective absolute value considerably below the vacuum value, as the parametrization for the case of $n_O = 14$ suggests, is not expected.

A further analysis of the results presented in Figure 3 shows that the slope of the vapor pressure line significantly changes with varying partial charge q_O. Figure 4 illustrates the deviations of calculated to experimental values. The errors in liquid density are less strongly changing (not shown), with a trend to lower errors for increasing partial charge q_O. The minimum in the objective function is therefore explained by an accurate representation of the vapor pressure line.

Other Alkyl Ethers. Diethyl ether and dipropyl ether are considered in this section. We strive to develop a transferable force field of the ether oxygen for these substances and for higher members of the homologous series. The concept of transferability is well established for Lennard-Jones parameters (or Mie parameters). For partial charges, the transferability has been assumed for some force fields, but this approximation is rather critical, as quantum chemical calculations suggest. We determined partial charges from the intrinsic atomic orbitals (IAO) approach[67] using a B3LYP functional with a def2-TZVPP basis set. The IAO partial charges are $q_O^{(IAO)} = -0.42$ and -0.42 for diethyl ether and dipropyl ether, respectively. The IAO charges resemble a chemical charge distribution rather than representing a molecules electrostatic field. We have seen the IAO charges to be weakly changing with molecule conformation. Further, as already pointed out in the work of Knizia,[67] the IAO charges are weakly dependent on the choice of the quantum mechanical approach. The electrostatic potential according to Besler et al. on the other hand more closely reflects an isolated molecules electrostatic field.[68] These charges are more dependent on the molecule conformation. From an automated force field topology builder,[69] we determined values of $q_O^{(ESP)} = -0.48$ and -0.52 for diethyl ether and dipropyl ether, respectively.

As the quantum chemical calculations suggest different partial charges for diethyl ether and for dipropyl ether, it is interesting to treat the charge as an adjustable parameter of the Mie force field. We expect that the parameter regression then also identifies different partial charges. Because static polarizability is not expected to have an exceedingly high contribution to the overall interactions of these two pure substances,[70] one would expect optimized partial charges close to the quantum mechanical values. In a first series of calculations, we varied the charges and optimized the two Mie potential parameters ϵ_O and σ_O separately for diethyl ether and dipropyl ether. Figures 5 and 6 show average deviations of the simulation results to the experimental values for vapor pressure and liquid densities for diethyl ether and dipropyl

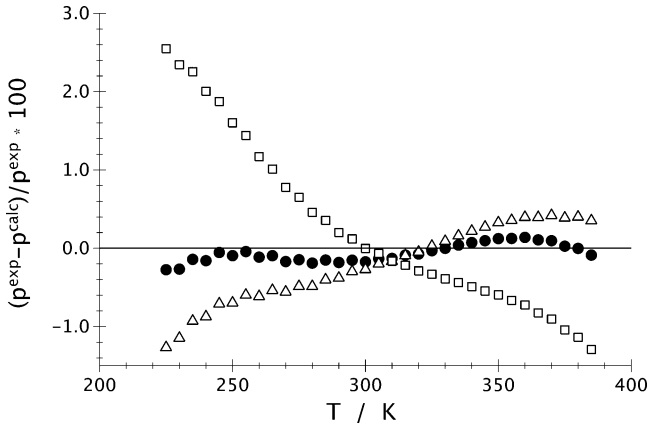

Figure 4. Dimethyl ether: Relative deviations (%) of simulated vapor pressure in comparison to experimental data. The temperature range corresponds to $0.56 \leq T/T_{crit}^{exp} \leq 0.96$. The symbols are for the case of $n_O = 12$ with a partial charge at the oxygen atom of $q_O = -0.32$ (squares), $q_O = -0.35$ (solid spheres), and $q_O = -0.36$ (triangles) all for optimized values of ϵ_O and σ_O.

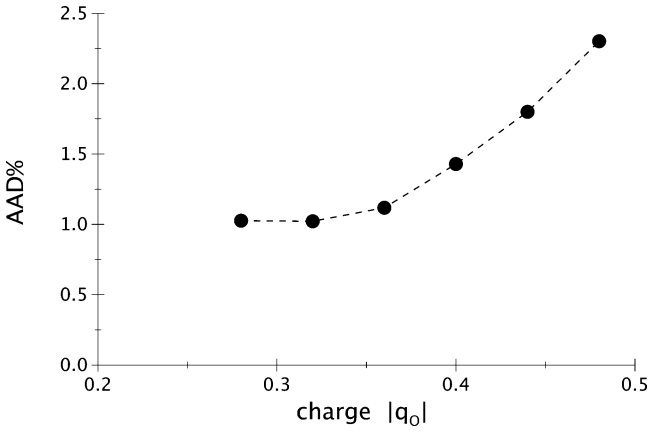

Figure 5. Diethyl ether: Absolute average deviations (%) of simulated vapor pressure and liquid density data to experimental data for varying partial charge q_O of the oxygen. The temperature range corresponds to $0.56 \leq T/T_{crit}^{exp} \leq 0.96$. For each symbol, the two parameters ϵ_O and σ_O (with $n_O = 12$) were optimized for diethyl ether only.

DOI: 10.1021/acs.jpcb.5b01806
J. Phys. Chem. B 2015, 119, 7087−7099

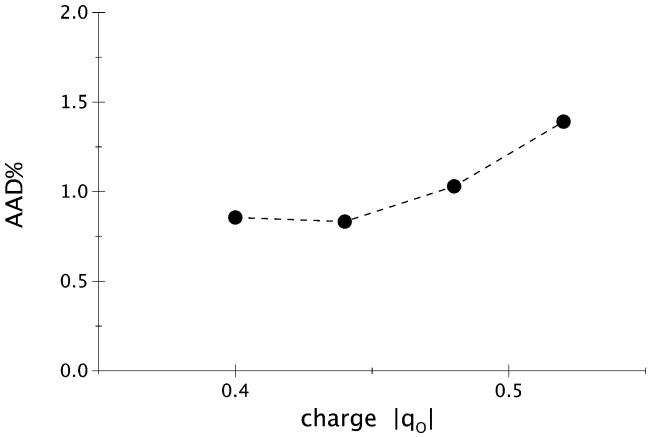

Figure 6. Dipropyl ether: Absolute average deviations (%) of simulated vapor pressure and liquid density data to experimental data for varying partial charge q_O of the oxygen. The temperature range corresponds to $0.53 \leq T/T_{crit}^{exp} \leq 0.96$. For each symbol, the two parameters ϵ_O and σ_O (with $n_O = 12$) were optimized for dipropyl ether only.

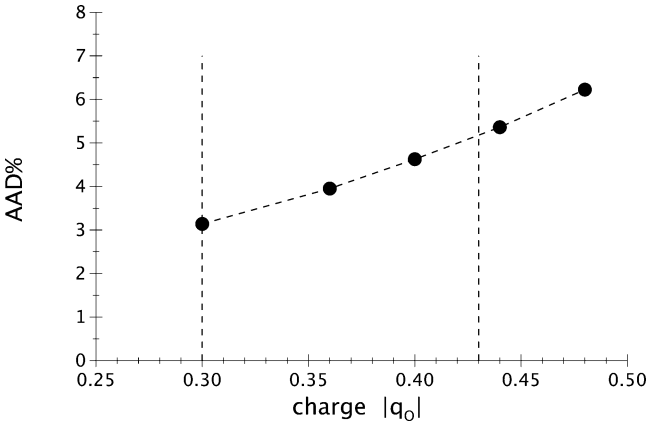

Figure 7. Simultaneous force field optimization for diethyl ether and dipropyl ether: Absolute average deviations (%) of simulated vapor pressure and liquid density data to experimental data for varying partial charge q_O of the oxygen. For each symbol, the two parameters ϵ_O and σ_O (with $n_O = 12$) were optimized.

ether, respectively. The Mie parameters ϵ_O and σ_O are optimized for each symbol in Figures 5 and 6. The rightmost value in both diagrams represents the partial charge suggested by quantum chemical calculations. The minima in Figures 5 and 6 of $q_O = -0.3$ for diethyl ether and $q_O = -0.43$ for dipropyl ether represent the optimal effective charge according to our parametrization. For these optimal effective partial charges, we find good agreement of the simulated vapor pressure curve and the liquid density curve to the experimental data, in the range of about 1% AAD, as the minima in Figures 5 and 6 indicate. We see, however, that the individually optimized value for diethyl ether is lower than the ones predicted for a vacuum from quantum mechanical calculations ($q_O^{(IAO)} = -0.42$), whereas the partial charge for dipropyl ether is in close agreement with the value from quantum mechanical estimates (also $q_O^{(IAO)} = -0.42$). The individual parameter regression has an important outcome: we obtained significantly different partial charges between the two members of the homologous series. That finding reveals limits for the concept of transferable partial charges.

Despite the critical assessment of the concept of transferable partial charges in our previous paragraph, we maintain the objective of developing transferable force fields. In a second series of simulations, we therefore optimized the two Mie potential parameters ϵ_O and σ_O simultaneously for diethyl ether and dipropyl ether. Figure 7 presents the deviations between molecular simulations and experimental data for varying partial charges. On the basis of the partial charges optimized individually to diethyl ether and dipropyl ether, we limited the range of partial charges to $q_O = -0.3$ and -0.43. These bounds were the optimal partial charge of diethyl ether and of dipropyl ether, respectively. Figure 7 shows that the best partial charge for a simultaneous parameter regression assuming transferable partial charges ends at the left bound. An unconstrained parameter regression would reveal partial charges lower than $|q_O| = 0.3$, i.e., lower than the value of either of the individually optimized values. We see no apposite argument for partial charges outside the range, constrained by the values found for individual optimizations. Lower partial charges would obviously lead to a better representation of pure components (Figure 7), but at the same time, it is likely that the predictive power for mixtures would then be sacrificed. We therefore adopt the partial charge of $q_O = -0.3$ for the TAMie force field. The parameters are summarized in Table 2.

Molecular simulations with the TAMie force field lead to satisfying agreement with the experimental data for diethyl ether and dipropyl ether, as Figures 8 and 9 show. These

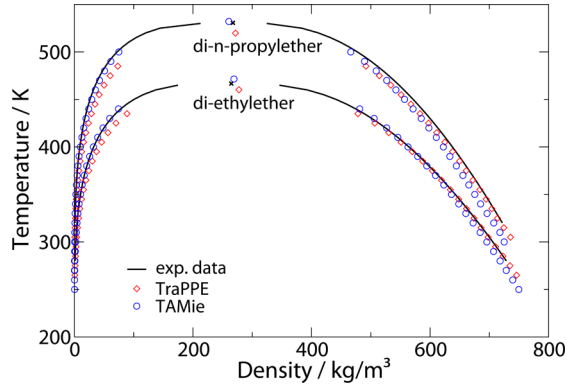

Figure 8. Vapor−liquid coexistence curve for short symmetric ether. Symbols are simulation results for the TAMie force field (blue spheres) and for the TraPPE model (red diamonds); solid lines are quasi-experimental data.[66]

diagrams also give a comparison to results of the TraPPE force field. Calculations using the TAMie parametrization sacrifice agreement with the liquid density data to a small extent but lead to a much better agreement with vapor pressure data compared with the TraPPE force field. The results in Figure 9 illustrate the observations discussed above: the partial charges of dipropyl ether are higher than diethyl ether, when the partial charge is individually optimized. Figure 9 shows that the vapor pressure for diethyl ether is calculated at too low values, whereas for diproyl ether the vapor pressure is overestimated. A single set of parameters (especially partial charges) for the ether oxygen is not sufficient to further reduce deviations to the experimental values.

Mixture. An important perspective for transferable force fields is the prediction of mixture properties. We investigate here the vapor−liquid equilibrium for a mixture of *n*-butane with dimethyl ether at $T = 405.16$ K. We first apply the TAMie

DOI: 10.1021/acs.jpcb.5b01806
J. Phys. Chem. B 2015, 119, 7087−7099

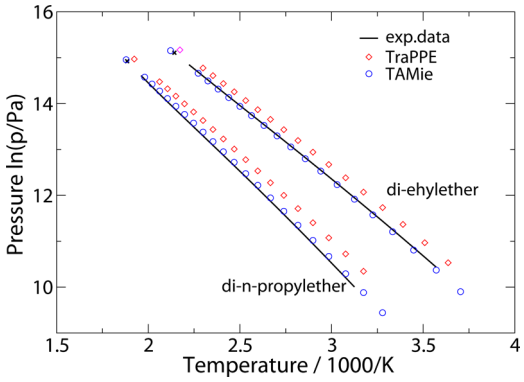

Figure 9. Vapor pressure curve for short symmetric ether. Symbols are simulation results for the TAMie force field (blue spheres) and for the TraPPE model (red diamonds); solid lines are quasi-experimental data.[66]

force field without correction parameters to the Berthelot–Lorentz combining rules, so that we can speak of a prediction. The comparison of the TAMie model (gray solid line) with experimental data is given in Figure 10. The TAMie force field

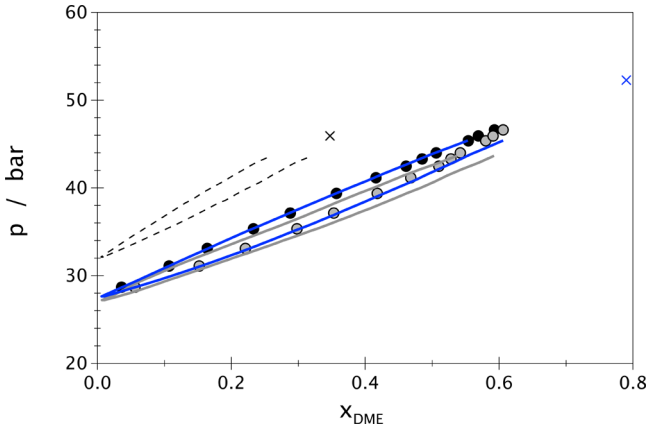

Figure 10. Vapor–liquid equilibrium for a mixture of *n*-butane/dimethyl ether (DME) at T = 405.16 K. Predictions from molecular simulation using the TAMie force field (solid line, gray) are compared to experimental data (symbols).[71] Results of the TAMie force field with binary interaction correction, $\kappa_{O,CHx}$ = 0.05 (solid line, blue). Predictions of the TraPPE model are also shown for comparison (dashed line). Estimates of the mixture critical points of the TAMie and the TraPPE force field are given as cross symbols.

reproduces the vapor pressure of pure *n*-butane with good accuracy. The slope of the bubble point line (and of the dew point line) as predicted from TAMie is somewhat too low. In view of the fact that no binary interaction parameter was adjusted, however, we consider the result of Figure 10 as a good overall agreement. The result suggests that the TAMie parameters are reasonably balanced.

The binary phase diagram can be improved when introducing a correction to the Berthelot rule, according to $\epsilon_{ij} = (\epsilon_{ii}\epsilon_{jj})^{1/2}(1 - \kappa_{ij})$. For like functional groups $i = j$, the correction parameter is $\kappa_{ij} = 0$. For the CH_3 groups and CH_2 groups of *n*-alkanes, we have seen no need for corrections, so that $\kappa_{CH_2,CH_3} = 0$. We have adjusted a symmetric intermolecular correction of the ether oxygen group $\kappa_{O,CH_x} = 0.05$, with $x \in \{2, 3\}$. Using this parameter, the simulation results are in excellent agreement with the experimental vapor–liquid equilibrium data, as the blue line in Figure 10 shows.

In Figure 10, we also added predictions of the TraPPE force field[59,61] for comparison. The TraPPE force field has its strength in the temperature–composition projections and reveals stronger deviations in the pressure–composition projection. From the comparison of the TAMie results to the TraPPE calculations, we wish to confirm that the TAMie model is in good agreement with the experimental data.

CONCLUSION

An analytical equation of state is used for defining conditions (chemical potentials, temperatures, and intervals of molecule number) of molecular simulations in the grand canonical ensemble in such a way that the phase envelopes of pure fluids are traced. Knowing these simulation conditions (approximately) prior to a molecular simulation in the grand canonical ensemble allows for a series of independent GCMC simulations conducted in parallel, leading to efficient parallel simulations that can be performed in a relatively short time using automated scripts.

We optimized parameters of the TAMie force field for describing phase equilibrium properties of ethers. We investigated whether the partial charge parameters representing the ether group and adjacent carbon (united-atom) groups are transferable for diethyl ether and dipropyl ether. We find that the individually optimized partial charges are quite different for these two ethers. It was seen that an unconstrained parameter optimization of a transferable force field adjusted simultaneously to both substances identifies partial charges smaller than each of the individually optimized partial charges. Our study suggests that partial charges should be constrained either to a range where individually optimized values lay or to a range obtained from quantum mechanical calculations.

ASSOCIATED CONTENT

Supporting Information

First, a summary of the calculation sequence for phase equilibrium calculations using histogram reweighting is given. Second, the robustness of the simulation method is assessed, by using artificially inaccurate estimates of (μ, T) from the PC-SAFT equation of state. The Supporting Information is available free of charge on the ACS Publications website at DOI: 10.1021/acs.jpcb.5b01806.

AUTHOR INFORMATION

Corresponding Author

*Phone: +49 (0)711 685 66103. Fax: +49 (0)711 685 66140. E-mail: gross@itt.uni-stuttgart.de.

Notes

The authors declare no competing financial interest.

ACKNOWLEDGMENTS

The authors thank the German Research Foundation (DFG) for financial support of the project within the Cluster of Excellence in Simulation Technology (EXC 310/2) at the University of Stuttgart. This work was performed on the computational resource bwUniCluster funded by the Ministry of Science, Research and Arts and the Universities of the State of Baden-Württemberg, Germany, within the framework program bwHPC. At Princeton, this work was supported by the Department of Energy, Office of Basic Energy Sciences,

DOI: 10.1021/acs.jpcb.5b01806
J. Phys. Chem. B 2015, 119, 7087–7099

under award DE-SC0002128. We much appreciate the help and guidance of Andreas Köhn (University of Stuttgart) on the quantum mechanical calculations. J.G. thanks Juan Manuel Castillo-Sanchez for helpful discussions.

REFERENCES

(1) de Pablo, J. J.; Yan, Q.; Escobedo, F. A. Simulation of phase transitions in fluids. *Annu. Rev. Phys. Chem.* **1999**, *50*, 377−411.
(2) Panagiotopoulos, A. Z. Monte Carlo methods for phase equilibria of fluids. *J. Phys.: Condens. Matter* **2000**, *12*, R25−R52.
(3) Binder, K. Computer simulations of critical phenomena and phase behaviour of fluids. *Mol. Phys.* **2010**, *108*, 1797−1815.
(4) Paluch, A. S.; Shen, V. K.; Errington, J. R. Comparing the use of Gibbs Ensemble and Grand-Canonical transition-matrix Monte Carlo methods to determine phase equilibria. *Ind. Eng. Chem. Res.* **2008**, *47*, 45233−4541.
(5) Ferrenberg, A. M.; Swendsen, R. H. New Monte Carlo technique for studying phase transitions. *Phys. Rev. Lett.* **1988**, *61*, 2635.
(6) Ferrenberg, A. M.; Swendsen, R. H. Optimized monte carlo data analysis. *Phys. Rev. Lett.* **1989**, *63*, 1195.
(7) Wilding, N. B. Critical-point and coexistence-curve properties of the Lennard-Jones fluid: a finite-size scaling study. *Phys. Rev. E* **1995**, *52*, 602.
(8) Panagiotopoulos, A. Z.; Wong, V.; Floriano, M. A. Phase equilibria of lattice polymers from Histogram Reweighting Monte Carlo simulations. *Macromolecules* **1998**, *31*, 9012−9018.
(9) Potoff, J. J.; Panagiotopoulos, A. Z. Critical point and phase behavior of the pure fluid and a Lennard-Jones mixture. *J. Chem. Phys.* **1998**, *109*, 10914−10920.
(10) Panagiotopoulos, A. Z. Monte Carlo Methods for phase equilibria of fluids. *J. Phys.: Condens. Matter* **2000**, *12*, R25−F52.
(11) Guevara-Carrion, G.; Hasse, H.; Vrabec, J. *Multiscale Molecular Methods in Applied Chemistry*; Springer: Berlin, 2012; pp 201−249.
(12) Smith, G. R.; Bruce, A. D. A study of the multi-canonical Monte Carlo method. *J. Phys. A: Math. Gen.* **1995**, *28*, 6623−6643.
(13) Wang, J.-S. Transition matrix Monte Carlo method. *Comput. Phys. Commun.* **1999**, *122*, 22−25.
(14) Wang, J.-S.; Tay, T. K.; Swendsen, R. H. Transition matrix Monte Carlo reweighting and dynamics. *Phys. Rev. Lett.* **1999**, *82*, 476−479.
(15) Fitzgerald, M.; Picard, R. R.; Silver, R. N. Canonical transition probabilities for adaptive Metropolis simulation. *Europhys. Lett.* **1999**, *46*, 282−287.
(16) Fitzgerald, M.; Picard, R. R.; Silver, R. N. Monte Carlo transition dynamics and variance reduction. *J. Stat. Phys.* **2000**, *98*, 321−345.
(17) Wang, J.-S.; Swendsen, R. H. Transition matrix Monte Carlo method. *J. Stat. Phys.* **2002**, *106*, 245−285.
(18) Shell, M. S.; Debenedetti, P. G.; Panagiotopoulos, A. Z. An improved Monte Carlo method for direct calculation of the density of states. *J. Chem. Phys.* **2003**, *119*, 9406−9411.
(19) Errington, J. R. Direct calculation of liquid-vapor phase equilibria from transition matrix Monte Carlo simulation. *J. Chem. Phys.* **2003**, *118*, 9915−9925.
(20) Fenwick, M. K.; Escobedo, F. A. On the use of Bennetts acceptance ratio method in multi-canonical-type simulations. *J. Chem. Phys.* **2004**, *120*, 3066−3074.
(21) Bennett, C. H. Efficient estimation of free energy differences from Monte Carlo data. *J. Comput. Phys.* **1976**, *22*, 245−268.
(22) Escobedo, F. A.; Abreu, C. R. A. On the use of transition-matrix method with extended ensemble. *J. Chem. Phys.* **2006**, *124*, 104110.
(23) Shi, W.; Maginn, E. J. Continuous fractional component Monte Carlo: An adaptive biasing method for open system atomistic simulations. *J. Chem. Theory Comput.* **2007**, *3*, 1451−1463.
(24) Shi, W.; Maginn, E. J. Atomistic simulation of the absorption of carbon dioxide and water in the ionic liquid 1-n-Hexyl-3-methylimidazolium Bis (trifluoromethylsulfonyl) imide ([hmim]-[Tf2N]. *J. Phys. Chem. B* **2008**, *112*, 2045−2055.
(25) Shen, V. K.; Errington, J. R. Determination of fluid-phase behavior using transition-matrix Monte Carlo: Binary Lennard-Jones mixtures. *J. Chem. Phys.* **2005**, *122*, 064508.
(26) Errington, J. R.; Shen, V. K. Direct evaluation of multi-component phase equilibria using flat histogram methods. *J. Chem. Phys.* **2005**, *123*, 164103.
(27) Sanchez, J. M. C.; Danner, T.; Gross, J. Grand canonical Monte Carlo simulations of vapor-liquid equilibria using a bias potential from an analytic equation of state. *J. Chem. Phys.* **2013**, *138*, 234106.
(28) Gross, J.; Sadowski, G. Perturbed-Chain SAFT: An equation of state based on a perturbation theory for chain molecules. *Ind. Eng. Chem. Res.* **2001**, *40*, 1244−1260.
(29) Gospodinov, I. D.; Escobedo, F. A. Bridging continuum and statistical thermodynamics via equations of state and the density of states. *J. Chem. Phys.* **2004**, *120*, 10699−10710.
(30) Gospodinov, I. D.; Escobedo, F. A. Probability density of macrostates and density of states for multi-component mixtures from semi-empirical equations of state. *Mol. Phys.* **2005**, *103*, 3115−3124.
(31) Lymperiadis, A.; Adjiman, C. S.; Galindo, A.; Jackson, G. A group contribution method for associating chain molecules based on the statistical associating fluid theory (SAFT-γ). *J. Chem. Phys.* **2007**, *127*, 234903.
(32) Lymperiadis, A.; Adjiman, C. S.; Jackson, G.; Galindo, A. A generalisation of the SAFT-group contribution method for groups comprising multiple spherical segments. *Fluid Phase Equilib.* **2008**, *274*, 85−104.
(33) Papaioannou, V.; Lafitte, T.; Avendaño, C.; Adjiman, C. S.; Jackson, G.; Müller, E. A.; Galindo, A. Group contribution methodology based on the statistical associating fluid theory for heteronuclear molecules formed from Mie segments. *J. Chem. Phys.* **2014**, *140*, 054107.
(34) Avendano, C.; Lafitte, T.; Galindo, A.; Adjiman, C. S.; Jackson, G.; Muller, E. A. SAFT-γ force field for the simulation of molecular fluids. 1. A single-site coarse grained model of carbon dioxide. *J. Phys. Chem. B* **2011**, *115*, 11154−11169.
(35) Avendan o, C.; Lafitte, T.; Adjiman, C. S.; Galindo, A.; Muller, E. A.; Jackson, G. SAFT-γ force field for the simulation of molecular fluids: 2. Coarse-grained models of greenhouse gases, refrigerants, and long alkanes. *J. Phys. Chem. B* **2013**, *117*, 2717−2733.
(36) Lafitte, T.; Avendaño, C.; Papaioannou, V.; Galindo, A.; Adjiman, C. S.; Jackson, G.; Müller, E. A. SAFT-γ force field for the simulation of molecular fluids: 3. Coarse-grained models of benzene and hetero-group models of n-decylbenzene. *Mol. Phys.* **2012**, *110*, 1189−1203.
(37) Müller, E. A.; Jackson, G. Force-field parameters from the SAFT-γ equation of state for use in coarse-grained molecular simulations. *Annu. Rev. Chem. Biomol. Eng.* **2014**, *5*, 405−427.
(38) Ucyigitler, S.; Camurdan, M. C.; Elliott, J. R. Optimization of transferable site-site potentials using a combination of stochastic and gradient search algorithms. *Ind. Eng. Chem. Res.* **2012**, *51*, 6219−6231.
(39) Sans, A.; Vahid, A.; Elliott, J. R. Transferable intermolecular potential models for a broad range of organic compounds. *J. Chem. Eng. Data* **2014**, *59*, 3069−3079.
(40) Ghobadi, A. F.; Elliott, J. R. Adapting SAFT-γ perturbation theory to site-based molecular dynamics simulation. I. Homogeneous fluids. *J. Chem. Phys.* **2013**, *139*, 234104.
(41) Ghobadi, A. F.; Elliott, J. R. Adapting SAFT-γ perturbation theory to site-based molecular dynamics simulation. II. Confined fluids and vapor-liquid interfaces. *J. Chem. Phys.* **2014**, *141*, 024708.
(42) v. Westen, T.; Vlugt, T. J. H.; Gross, J. Determining force field parameters using a physically based equation of state. *J. Phys. Chem. B* **2011**, *115*, 7872−7880.
(43) Hemmen, A.; Gross, J. Transferable anisotropic united-atom force field based on Mie potential for phase equilibrium calculations: n-akanes and n-olefins. *J. Phys. Chem. B* **2015**, submitted.
(44) Virnau, P.; Müller, M. Calculation of free energy through successive umbrella sampling. *J. Chem. Phys.* **2004**, *120*, 10925−10930.

DOI: 10.1021/acs.jpcb.5b01806
J. Phys. Chem. B 2015, 119, 7087−7099

(45) Wilding, N. B.; Müller, M. Liquid-vapor asymmetry in pure fluids: A Monte Carlo simulation study. *J. Chem. Phys.* **1995**, *102*, 2562−2573.
(46) Wilding, N. B. Simulation studies of fluid critical behavior. *J. Chem. Phys.* **1997**, *9*, 585−612.
(47) Binder, K. Finite size scaling analysis of Ising model block distribution functions. *Z. Phys. B: Condens. Matter* **1981**, *43*, 119−140.
(48) Perez-Pellitero, J.; Ungerer, P.; Orkoulas, G.; Mackie, A. D. Critical point estimation of the Lennard-Jones pure fluid and binary mixtures. *J. Chem. Phys.* **2006**, *125*, 054515.
(49) Ferrenberg, A. M.; Landau, D. P. Critical behavior of the tree-dimensional Ising model: A high-resolution Monte Carlo study. *Phys. Rev. B* **1991**, *44*, 5081−5091.
(50) Binder, K.; Luijten, E. Monte Carlo tests of renormalization-group predictions for critical phenomena in Ising models. *Phys. Rep.* **2001**, *344*, 179−253.
(51) Toxvaerd, S. Molecular Dynamics calculation of the equation of state of alkanes. *J. Chem. Phys.* **1990**, *93* (6), 4290−4295.
(52) Errington, J. R.; Panagiotopoulos, A. Z. A new intermolecular potential model for the n-alkane homologous series. *J. Phys. Chem. B* **1999**, *103*, 6314−6322.
(53) Ungerer, P.; Beauvais, C.; Delhommelle, J.; Boutin, A.; Rousseau, B. Optimization of the anisotropic united atoms intermolecular potential for n-alkanes. *J. Chem. Phys.* **2000**, *112*, 5499−5510.
(54) Potoff, J. J.; Bernard-Brunel, D. A. Mie potentials for phase equiilbria calculations: Application to alkanes and perfluoralkanes. *J. Phys. Chem. B* **2009**, *113*, 14725−14731.
(55) Potoff, J. J.; Kamath, G. Mie potentials for phase equilibria: Application to alkenes. *J. Chem. Eng. Data* **2014**, *59*, 3144−3150.
(56) Lorentz, H. A. Über die Anwendung des Satzes vom Virial in der kinetischen Gastheorie. *Ann. Phys.* **1881**, *12*, 127−136.
(57) Berthelot, D. C. R. Sur le Mélange des Gaz. *C. R. Acad. Sci.* **1898**, *126*, 1703−1855.
(58) Stiegler, T.; Sadus, R. J. Molecular simulation of fluids with non-identical intermolecular potentials: Thermodynamic properties of 10−5+ 12−6 Mie potential binary mixtures. *J. Chem. Phys.* **2015**, *142*, 084504.
(59) Martin, M. G.; Siepmann, J. I. Transferable potentials for phase equilibria. 1. United-atom description of n-alkanes. *J. Phys. Chem. B* **1998**, *102*, 2569−2577.
(60) Jorgensen, W. L.; Madura, J. D.; Swenson, C. J. Optimized intermolelcular potential functions for liquid hydrocarbons. *J. Am. Chem. Soc.* **1984**, *106*, 6638−6646.
(61) Stubbs, J. M.; Potoff, J. J.; Siepmann, J. I. Transferable potential for phase equilibria. 6. United-atom description for ethers, glycols, ketones, and aldehydes. *J. Phys. Chem. B* **2004**, *108*, 17596−17605.
(62) Allen, M. P.; Tildesley, D. J. *Computer simulation of liquids*; Oxford Science Publications: Oxford, 1987.
(63) d. Ploeg, P. V.; Berendsen, H. J. C. Molecular dynamics simulation of a bilayer membrane. *J. Chem. Phys.* **1982**, *76*, 3271−3276.
(64) Smit, B. Phase diagrams of LennardJones fluids. *J. Chem. Phys.* **1992**, *96*, 8639−8640.
(65) Ketko, M. H.; Potoff, J. J. Effect of partial charge parameterization on the phase equilibria of dimethyl ether. *Mol. Simul.* **2007**, *33*, 769−776.
(66) Rowley, R. L.; Wilding, W. V.; Oscarson, J. L.; Yang, Y.; Zundel, N. A.; Daubert, T. E.; Danner, R. P. DIPPR data compilation of pure chemical properties. Design Institute for Physical Properties, AIChE: New York, NY, 2009.
(67) Knizia, G. Intrinsic atomic orbitals: An unbiased bridge between quantum theory and chemical concepts. *J. Chem. Theory Comput.* **2013**, *9*, 4834−4843.
(68) Besler, B. H.; Merz, K. M.; Kollman, P. A. Atomic charges derived from semiempirical methods. *J. Comput. Chem.* **1990**, *11*, 431−439.
(69) Malde, A. K.; Zuo, L.; Breeze, M.; Stroet, M.; Poger, D.; Nair, P. C.; Oostenbrink, C.; Mark, A. E. An automated force field topology builder (ATB) and repository: version 1.0. *J. Chem. Theory Comput.* **2011**, *7*, 4026−4037.
(70) Kleiner, M.; Gross, J. An equation of state contribution for polar components: Polarizable dipoles. *AIChE J.* **2006**, *52*, 1951−1961.
(71) de Fernandez, M. E. P.; Calado, J. C. G.; Streett, W. B. Vapor-liquid equilibria in the binary system dimethyl ether+ n-butane from 282.9 to 414.5 K at pressures to 4.82 MPa. *Fluid Phase Equilib.* **1992**, *74*, 289−302.

DOI: 10.1021/acs.jpcb.5b01806
J. Phys. Chem. B 2015, 119, 7087−7099